Inorganica Chimica Acta 375 (2011) 20–30

Contents lists available at ScienceDirect

Inorganica Chimica Acta

journal homepage: www.elsevier.com/locate/ica

Preferential azido bridging regulating the structural aspects in cobalt(III) and copper(II)–Schiff base complexes: Syntheses, magnetostructural correlations and catalytic studies

Aurkie Ray [a], Georgina M. Rosair [b], Guillaume Pilet [c], Bülent Dede [d], Carlos J. Gómez-García [e], Sandra Signorella [f], Sebastián Bellú [f], Samiran Mitra [a,*]

[a] Department of Chemistry, Jadavpur University, Raja S.C. Mullick Road, Kolkata 700 032, India
[b] School of Engineering and Physical Sciences, Heriot Watt University, Edinburgh EH14 4AS, UK
[c] Groupe de Cristallographie et Ingénierie Moléculaire Laboratoire des Multimatériaux et Interfaces UMR 5615 CNRS, Université Claude Bernard Lyon 1, Bât. Jules Raulin, 43 bd du 11 Novembre, 1918 69622 Villeurbanne, Cedex, France
[d] Department of Chemistry, Faculty of Arts and Sciences, Süleyman Demirel University, Isparta, Turkey
[e] Instituto de Ciencia Molecular (ICMol), Universidad de of Valencia, Parque Científico, 46980 Paterna, Spain
[f] Instituto de Química Rosario (IQUIR), CONICET, Facultad de Ciencias Bioquímicas y Farmacéuticas, Universidad Nacional de Rosario, Suipacha 531, S2002LRK Rosario, Argentina

ARTICLE INFO

Article history:
Received 5 November 2010
Received in revised form 14 March 2011
Accepted 4 April 2011
Available online 9 April 2011

Keywords:
$\mu_{1,1}$-, $\mu_{1,1,1}$-, $\mu_{1,3}$-Azide
M = Co^{III}, Cu^{II}
Schiff base
Crystal structures
VTM
Alkene oxidation

ABSTRACT

A tridentate NNO donor Schiff base ligand [(1*Z*,3*E*)-3-((pyridin-2-yl)methylimino)-1-phenylbut-1-en-1-ol = **LH**] in presence of azide ions coordinates with cobalt(II) and copper(II) ions giving rise to three new coordination complexes $[Co_2(\mathbf{L})_2(\mu_{1,1}\text{-}N_3)_2(N_3)_2]$ (**1**), $[Cu_2(\mathbf{L})_2(\mu_{1,3}\text{-}N_3)]\cdot ClO_4$ (**2**) and $[(\mu_{1,1}\text{-}N_3)_2Cu_5(\mu\text{-}O\mathbf{L})_2(\mu_{1,1}\text{-}N_3)_4(\mu_{1,1,1}\text{-}N_3)_2]_n$ (**3**). The complexes have been characterized by elemental analysis, FT-IR, UV–Vis spectral studies, and single crystal X-ray diffraction studies. These complexes demonstrate that under different synthetic conditions the azide ions and the Schiff base ligand (**LH**) show different coordination modes with cobalt(II) and copper(II) ions, giving rise to unusual dinuclear and polynuclear species (**1**, **2** and **3**) whose structural variations are discussed. Magneto-structural correlation for the very rare singly $\mu_{1,3}$-N_3 bridged Cu^{II}–Schiff base dinuclear species (**2**) has been studied. In addition, the catalytic properties of **1** for alkene oxidation and the general catalase-like activity behavior of **2** have been discussed.

1. Introduction

The major task in designing pseudohalide bridged compounds depends on the proper choice of the bridging ligands as well as the stereochemical environment surrounding the paramagnetic centers. The azide ion has been shown to be able to link two or more metal ions in various modes: where μ-1,1 (*end-on*, EO) and μ-1,3 (*end-to-end*, EE) are the usual modes but not the only, since other modes, including μ_3-1,1,1 [1], μ_4-1,1,1,1 [2], μ_3-1,1,3 [3], or the very rare μ_4-1,1,3,3 [4] modes have also been observed. The azide ligand has been a prominent actor in the development of molecular magnetism since its inception [5]. Primarily, this group has acted as a structural bridge and magnetic coupler of paramagnetic metal ions within one-, two- or three-dimensional extended coordination arrays, rather than discrete molecules, unveiling interesting phenomena such as ferrimagnetism within homometallic chains [6], or sheets [7].

Regarding the magnetic coupling, it is well known that azide ions with a symmetric μ-1,1 (*end-on*, EO) coordination mode, give rise to ferromagnetic coupling as far as the Cu–N–Cu angle does not exceeds ca. 104° [8]. On the other hand, for the symmetric μ-1,3 (*end-to-end*, EE) coordination mode, the magnetic coupling is strong and antiferromagnetic [9]. Interestingly, for asymmetric azide bridges, the coupling is weak and antiferromagnetic except for the EE coordination mode with a long Cu–N bond distance that may give rise to a weak ferromagnetic coupling [10]. The huge number of azide cooper(II) complexes [11–21] have lead to several theoretical and magneto-structural correlations where different structural parameters as (i) the Cu–N bond distances, (ii) the Cu–N–Cu bond angles, (iii) the asymmetry of the bridge and (iv) the torsion angle in the central Cu_2N_2 entity have been considered [8–10,22].

Unlike the doubly *end-to-end* azido bridged copper(II) dinuclear species, singly *end-to-end* azido bridged copper(II) dinuclear complexes are still very rare [23–27]. In theses rare examples the coupling is much weaker than in the doubly *end-to-end* azido bridge copper(II) complexes, where antiferromagnetic interactions as strong as $-105\ cm^{-1}$ have been found [20].

* Corresponding author. Tel.: +91 33 2414 6666x2779; fax: +91 33 2414 6414.
E-mail address: smitra_2002@yahoo.com (S. Mitra).

0020-1693/$ - see front matter © 2011 Elsevier B.V. All rights reserved.
doi:10.1016/j.ica.2011.04.008

Many Schiff base complexes of metal ions show high catalytic activity. The oxidation of hydrocarbons using Schiff base complexes has been a field of academic and industrial interest to analyze the catalytic activity of various metal complexes [28–32]. The ring opening of large cycloalkanes is usually a difficult process but Schiff base complexes of cobalt(II) [33] and chromium(III) [34] were effective in these reactions with significant enantioselectivity. The manganese(II) complexes of bis(2-pyridinaldehyde)-ethylenediamine and bis(2-pyridinaldehyde)-propylenediamine ligands have been used in epoxidation of olefins but reasonable epoxide selectivity was possible only in the presence of PhIO oxidant [35]. The extent of olefins epoxidation was dependent on OH substitution on the Schiff base ligand. The enantioselective epoxidation of styrene, indene and 2,2-dimethyl-6-nitro chromene has been carried out using dicationic chiral manganese(III) salen complexes [36]. It has also been found that the epoxidation of styrene to styrene oxide with yields as high as 96% has been achieved by poly-(vinylbenzyl)acetylacetonate complexes of cobalt(II) or manganese(II) in the presence of isobutyraldehyde under an atmospheric pressure of molecular oxygen at room temperature [37]. Interestingly no other azido-bridged dicobalt complex has been tested previously for alkene oxidation. Besides, most cobalt complexes previously tested for the oxidation of alkenes with several oxidants, required large amounts of catalyst and afforded low t.o.n. In this sense, the study of the catalytic activity of new cobalt complexes with different topology and ligands provides some clues for the design of more efficient catalysts.

Recently, the reactivity of both homo- and hetero-polynuclear copper(II)–Schiff base complexes for H_2O_2 disproportionation, as a functional model for Mn-CAT has been investigated [38]. Catalase, one of the three major sensitive protective enzymes in living organisms, exists in almost all aerobically respiring organisms. It protects cells from the toxic effects of hydrogen peroxide (H_2O_2), the latter being linked to a variety of pathological consequences such as aging, diabetes and cancer [39–41]. On the other hand hydrogen peroxide is a ubiquitous metabolite in living systems, produced at increased levels in a variety of pathological situations. All living cells have devised a sophisticated machinery to suppress or at least control H_2O_2 production. The catalase enzymes which are able to disproportionate H_2O_2 into less harmful dioxygen and water are an important part of this machinery (Eq. (1)).

$$2H_2O_2 \rightarrow 2H_2O + O_2 \quad (1)$$

The $HO^{\cdot}/HOO^{\cdot}$ radical formation induces lipid peroxidation, membrane damage, and cell death [42]. In normal conditions, the organism protects itself against hydrogen peroxide using the catalase enzyme. However, when a stress occurs, the natural defenses are insufficient [42]. Because the natural enzyme cannot be used as a drug due to its instability in solution and to delivery problems, synthetic compounds able to dismutate hydrogen peroxide have been designed and studied [43–46].

In this paper we present three new azido complexes $[Co_2(\mathbf{L})_2(\mu_{1,1}\text{-}N_3)_2(N_3)_2]$ (**1**), $[Cu_2(\mathbf{L})_2(\mu_{1,3}\text{-}N_3)].ClO_4$ (**2**) and $[(\mu_{1,1}\text{-}N_3)_2Cu_5(\mu\text{-}O\mathbf{L})_2(\mu_{1,1}\text{-}N_3)_4(\mu_{1,1,1}\text{-}N_3)_2]_n$ (**3**), exhibiting the μ-1,1 (*end-on*, EO), μ-1,3 (*end-to-end*, EE) and the unprecedented μ_3-1,1,1 coordination modes of azide ions with a tridentate NNO donor Schiff base ligand (**LH**) [47]. Single crystal X-ray diffraction study revealed that, **1** (brown needle-shaped crystals) is a symmetrical double $\mu_{1,1}$-azido bridged cobalt(III) dinuclear complex whereas **2** (brown prismatic crystals) is a unique copper(II) dimer with a single symmetric $\mu_{1,3}$-azido bridge. By changing the molar ratio of the copper salt, the Schiff base ligand (**LH**) and the azide ion we have also obtained a dark blue amorphous product in much lower yield (compared to that of **2**) whose recrystallisation yielded a few blue needle-shaped single crystals of **3**. The X-ray diffraction study of **3** shows the presence of enolato bridges along with μ-1,1 and the rare μ_3-1,1,1 bridging modes of azide ions resulting in the formation of a new copper(II) coordination polymer, composed of vertex shared dicubanes with a vacant vertex. All the complexes were characterized by elemental analysis, FT-IR, UV–Vis spectroscopies. Variable temperature magnetic susceptibility measurement was performed only for **2** since **1** is diamagnetic (dinuclear Co^{III} species) and **3** was obtained in a much lower yield even after several attempts of its synthesis. Finally, we have also measured the catalytic properties of **1** for alkene oxidations and the general catalase-like activity behavior for **2**.

2. Experimental

2.1. Materials

Benzoylacetone and 2-picolylamine were purchased form Aldrich Chemical Company. Sodium azide was purchased from Fluka and were used as received. Cobalt perchlorate hexahydrate and copper perchlorate hexahydrate were prepared by treatment of the respective metal carbonates (cobalt carbonate and copper carbonate (E. Merck, India)) with 60% perchloric acid (E. Merck, India) followed by the slow evaporation on a steam bath. Thereafter filtered through a fine glass-frit and were preserved in a $CaCl_2$ desiccator for further use. Styrene, *cis*-stylbene, cyclohexene, *trans*-4-octene, *m*-chloroperbenzoic acid (*m*-CPBA), *N*-methylmorpholine *N*-oxide (NMO) and 4-phenyl pyridine *N*-oxide (PNO) used in the catalytic experiments were purchased from Aldrich and used as received. Dichloromethane, acetonitrile and acetone were of HPLC grade (Merk). Iodosylbenzene (PhIO) was synthesized using reported procedures by hydrolysis of iodobenzene diacetate with a solution of sodium hydroxide [48]. Styrene oxide and benzaldehyde used to obtain HPLC calibration curves were purchased from Aldrich. The concentration of H_2O_2 stock solution was determined by iodometric titration. O_2 saturated Cl_2CH_2 or CH_3CN solutions were used for oxidation assays where O_2 was the oxygen source.

2.2. Physical measurements

The Fourier Transform Infrared spectra (4000–400 cm^{-1}) of the ligand and the complexes were recorded on a Perkin–Elmer Spectrophotometer RX I FT-IR system as solid KBr pellets. The electronic spectra of the ligand and complexes were recorded at 300 K on a Perkin–Elmer λ – 40 UV–Vis-spectrometer using HPLC grade acetonitrile as solvent with a 1 cm quartz cuvette in the range 200–800 nm. C, H, N microanalyses of the ligand and the complexes were carried out with a Perkin-Elmer 2400 II elemental analyser. The magnetic susceptibility measurements were carried out in the temperature range 2–300 K with an applied magnetic field of 0.1 T on a polycrystalline sample of **2** with a Quantum Design MPMS-XL-5 SQUID magnetometer. The susceptibility data were corrected for the sample holders previously measured using the same conditions and for the diamagnetic contributions of the salt as deduced by using Pascal's constant tables. HPLC experiments were performed with a Varian ProStar chromatograph equipped with DAD 335 detector using a Varian Microsorb-MV 100-5 C18 column (250 × 4.6 mm), thermostated with a Zeltec heater. Samples were eluted with a 70:30 acetonitrile:methanol mixture at 40 °C and a flow rate of 0.4 mL/min. Under these experimental conditions, retention times (R_t) were: styrene (R_t = 7.92 min), styrene epoxide (R_t = 7.21 min), benzaldehyde (R_t = 7.05 min), *cis*-stylbene (R_t = 8.51 min), cyclohexene (R_t = 9.47 min), *trans*-4-octene (R_t = 11.39 min), *m*-chloroperbenzoic acid (R_t = 7.20 min) and iodosylbenzene (R_t = 8.45 min). Calibration curves were used to quantify the alkene conversion and product selectivity. At least two independent experiments were performed for each reaction condition. Blank experiments with each

oxidant and using the same experimental conditions except catalyst were performed. In every case, alkene conversion was null (PhIO + alkene reaction) or much slower than in the presence of the complex.

2.3. Synthesis

2.3.1. Synthesis of $[C_6H_5C(OH)=CHC(CH_3)=NCH_2C_5H_4N]$ (**LH**)

The synthesis and characterization of the Schiff base ligand (**LH**) has been done following the method described in the literature [47]. The 1:1 equimolar condensation of 2-picolylamine and benzoylacetone for 2 h in methanolic medium results in a yellow solution. The color indicates the formation of the Schiff base ligand (**LH**) which was used without further purification. Yield: 0.221 g (88%). *Anal.* Calc. for $[C_{16}H_{16}N_2O]$: C, 76.19; H, 6.35; N, 11.11. Found: C, 76.18; H, 6.31; N, 11.10%.

Caution! Perchlorate salts and azide derivatives in presence of organic ligands are potentially explosive and should be used in small quantity with much care.

2.3.2. Syntheses of $[Co_2(\mathbf{L})_2(\mu_{1,1}\text{-}N_3)_2(N_3)_2]$ (**1**)

The slow addition of 20 mL of a yellow methanolic solution of the Schiff base (**LH**) (0.252 g, 1 mmol) to 10 mL of a methanolic solution of cobalt perchlorate hexahydrate (0.365 g, 1 mmol) resulted in a dark red solution. This solution was stirred for 15 min at room temperature and then followed by the addition of 2 mL of an aqueous solution of sodium azide (0.130 g, 2 mmol). The dark red solution so obtained was gently stirred for 1 h at 40 °C, resulting in a color change from dark red to dark brown. The dark brown solution was then filtered and kept at room temperature. Brown needle shaped crystals suitable for X-ray diffraction was obtained after one day. The crystals were filtered and air-dried. Yield: 0.314 g (86%). *Anal.* Calc. for $[C_{32}H_{30}\ Co_2N_{16}O_2]$: C, 48.69; H, 3.80; N, 28.40. Found: C, 48.62; H, 3.77; N, 28.38%.

2.3.3. Syntheses of $[Cu_2(\mathbf{L})_2(\mu_{1,3}\text{-}N_3)]\cdot ClO_4$ (**2**)

Copper perchlorate hexahydrate (0.37 g, 1 mmol) was dissolved in 10 mL of methanol by stirring. It was then followed by the subsequent addition of 20 mL of a yellow methanolic solution of **LH** (0.252 g, 1 mmol) resulting in a light green solution. While the solution was stirred, 5 mL of an aqueous methanolic solution of sodium azide (0.032 g, 0.5 mmol) were carefully added dropwise to the light green solution to give a dark green solution. Addition of sodium azide was immediately stopped when a small amount of brown colored solid separated. The dark green solution was then filtered and kept in a refrigerator. Brown prismatic crystals suitable for X-ray diffraction were obtained after three days. Crystals were filtered and air-dried. Yield: 0.303 g (82%). *Anal.* Calc. for $[C_{32}H_{30}Cl_1Cu_2N_7O_6]$: C, 49.79; H, 3.89; N, 12.70. Found: C, 49.78; H, 3.85; N, 12.68%.

2.3.4. Syntheses of $[(\mu_{1,1}\text{-}N_3)_2Cu_5(\mu\text{-}O\mathbf{L})_2(\mu_{1,1}\text{-}N_3)_4(\mu_{1,1,1}\text{-}N_3)_2]_n$ (**3**)

Copper perchlorate hexahydrate (0.55 g, 1.5 mmol) was dissolved in 1:1 v/v methanol–acetone mixture (20 mL) by vigorous stirring. 10 mL of a yellow methanolic solution of the Schiff base (**LH**) (0.126 g, 0.5 mmol) were slowly added with stirring to the copper perchlorate hexahydrate solution to produce a bluish green solution. Successive very slow addition of 5 mL of an aqueous solution of sodium azide (0.192 g, 3 mmol) at higher molar ratio compared to that of **2**, prevented the precipitation of a brown solid and resulted in a dark green solution that produced a small amount of green solid which redissolved upon complete addition of sodium azide. The obtained dark green solution was then filtered and was kept at room temperature. A dark blue amorphous product was obtained in a much lower yield (compared to that of **2**) after a week. Recrystallisation of the dark blue product in 1:1 v/v methanol–acetonitrile mixture resulted in a few blue needle shaped single crystals suitable for X-ray diffraction after two weeks. Crystals were filtrated and air-dried. The IR spectra of the amorphous and the crystalline product were almost similar to each other but were not superimposable. Yield: 0.165 g (30%). *Anal.* Calc. for $[C_{32}H_{30}Cu_5N_{28}O_2]$: C, 33.20; H, 2.59; N, 33.89. Found: C, 33.18; H, 2.53; N, 33.86%.

2.4. Crystallographic data collections and structure determinations

The crystal structure analyses of **1**, **2** and **3** were performed using three different X-ray diffractometers. The equipment used for each sample is listed with the crystallographic data and the refinement results in Table 1. Single crystals of **1**, **2** and **3** were coated in Paratone-N heavy oil and mounted in a Cryoloop before being transferred to the cold stream on the respective diffractometers. The structure of **1** has been solved by direct methods using the SIR92 program [49] combined to fourier difference syntheses and refined against F using reflections with $[I > 2\sigma(I)]$ with CRYSTALS program [50]. The H atoms for **1** were all located in a difference map, but those attached to carbon atoms were repositioned geometrically. For **2** a semi-empirical absorption correction MULTISCAN program [51] has been applied to the data sets. Structure solution and refinement have been performed by using SHELXS-97 and SHELXL-97 programs [52,53]. For **3** data collection, reduction and absorption corrections were done with the APEX2 suite of programs [54]. All non hydrogen atoms were refined with anisotropic displacement parameters. All hydrogen atoms were located in calculated positions to correspond to standard bond lengths and angles.

2.5. Catalysis experiments

2.5.1. Procedure for alkene oxidations

Complex **1** (1 μmol (0.2 mol%) and 20 μmol (4 mol%)) and an olefin substrate (0.5 mmol) were dissolved in freshly distilled specified solvent (CH_2Cl_2, CH_3CN or acetone). With stirring and at a controlled temperature the oxidant (1 mmol in oxidation with PhIO and *m*-CPBA, 5 mmol in oxidation with aqueous 30% H_2O_2, and O_2 saturated solution with dioxygen) was added. Then the reaction was stirred at constant temperature and the reaction time for maximal conversion was determined by withdrawing periodically aliquots of 20 μL from the reaction mixture. This time was used to monitor the efficiency of the catalyst. Parallel experiments were carried out by dissolving a neutral donor ligand (NMO and PNO, 0.5 mmol) together with **1** + alkene. Aliquots were diluted with 2 mL of acetonitrile and filtered through a 0.2 μm membrane prior to injection into the chromatograph.

2.5.2. Procedure for catalase-like activity

Volumetric measurements of evolved dioxygen during the reactions of the dinuclear copper(II) complex (**2**) with H_2O_2 were carried out as follows:

A 50 cm^3 three-necked round-bottom flask containing a DMF solution of the complex (2 mL, 1 mM) was placed in a water bath (25 °C). One of the necks was connected to a burette and the others were stoppered by a rubber septum. While the solution was stirring, H_2O_2 (0.5 mL, 3.08 M) was injected into it through the rubber septum using a microsyringe. Volumes of evolved dioxygen were measured at 1 min time intervals by volumetry. In cases where imidazole, 1-methylimidazole or pyridine (0.5 mL) was added this was introduced into the reaction vessel before the addition of H_2O_2 (in the absence of the base the complex was either inactive or very weak catalysts for this reaction).

Table 1
Crystallographic and refinement data for **1**, **2** and **3**.

Complex	**1**	**2**	**3**
Diffractometer used	Nonius Kappa CCD	Rigaku Saturn	Bruker X8 Apex 2
Radiation type	graphite monochromatised Mo Kα	graphite monochromatised Mo Kα	graphite monochromatised Mo Kα
Radiation wavelength (Å)	0.71073	0.71070	0.71073
Empirical formula	$C_{32}H_{30}Co_2N_{16}O_2$	$C_{32}H_{30}Cl_1Cu_2N_7O_6$	$C_{32}H_{30}Cu_5N_{28}O_2$
Formula weight	788.56	771.18	1156.57
Crystal size (mm)	0.05 × 0.05 × 0.16	0.20 × 0.20 × 0.40	0.35 × 0.16 × 0.08
Crystal system	monoclinic	monoclinic	monoclinic
Space group	$P2_1/c$ (No. 14)	$C2/c$ (No. 15)	$C2/c$ (No. 15)
Crystal color	brown	brown	blue
Z	2	4	4
a (Å)	8.9994(8)	7.818(1)	21.916(3)
b (Å)	22.823(2)	15.889(2)	11.9560(14)
c (Å)	9.3132(5)	26.593(4)	19.004(2)
α (°)	90	90	90
β (°)	115.604(3)	106.682(2)	124.110(3)
γ (°)	90	90	90
V (Å^3)	1725.0(2)	3164.4(7)	4122.8(8)
T (K)	293	293(2)	100(2)
Density (Mg/m^3)	1.518	1.619	1.860
Absorption coefficient (mm^{-1})	1.019	1.486	2.610
F(0 0 0)	808	1576	2308
θ Range for data collection (°)	1.8–25.4	2.9–26.0	2.24–31.73
Reflections collected	5416	10 551	27 619
Independent reflections, (R_{int})	2914, 0.080	3023, 0.018	6548, 0.0454
Number of 'observed' reflections	1022	2848	4703
Goodness-of-fit (GOF), S	1.19	1.05	0.976
Final R indices [$I > 2\sigma(I)$]	R_1 = 0.0424 wR_2 = 0.0790	R_1 = 0.0403 wR_2 = 0.1064	R_1 = 0.0415 wR_2 = 0.0963
Largest difference in peak and hole (e Å^{-3})	0.33 and −0.26	0.55 and −0.51	1.168 and −0.759

2.5.3. Preparation of the haemolysate

Blood from different five human collected in EDTA (20–25 years old healthy male) was centrifuged (15 min, 2500g). Preparation of the haemolysate was done as described by Ninfali [55].

CAT activity was determined with the following procedure. 40 μL of the haemolysate was added to a tube containing 1000 μL of sodium phosphate buffer saline (PBS, 0.01 M, pH 7.4), and 1000 μL of 9.7 M H_2O_2 (dissolved in sodium phosphate buffer) and 20 μL of **2** (1 mM) was added to start the reaction. Evolved dioxygen (mL) was recorded following the reduction of hydrogen peroxide during 3 min by volumetry. All statistical analyses were performed using Statistica software release 6.0. Analysis of variance was performed and means were separated using Fisher's protected least significant differences (LSD) test at $P \leqslant 0.05$.

3. Results and discussion

3.1. Fourier Transform IR spectroscopy

The IR spectra of **1**, **2** and **3** have been analyzed in comparison with that of the free ligand **LH** in the region 4000–400 cm^{-1}. Although derived from the same Schiff base ligand (**LH**); the IR spectra of **1**, **2** and **3** are quite different from one another except the characteristic IR bands for the azide ligand centered in the region 2022–2084 cm^{-1} for all three complexes. In the spectra of **1**, **2** and **3** well resolved sharp bands with a bifurcated peak at 2057, 2022 (**1**), 2078, 2068 (**2**) and 2084, 2050 (**3**) cm^{-1} are observed and assigned to $\nu_{N=N}$ stretching of the azide moiety coordinated to different metal centers simultaneously [56,57]. The characteristic imine stretching band at 1624 cm^{-1} for **LH** has been considerably shifted to lower frequencies 1609 (**1**) and 1610 (**2**) and 1612 (**3**) cm^{-1} in the spectra of the complexes, and thereby clearly indicate coordination of the imine nitrogen with the metal centers in the respective complexes. Moreover, in the spectra of the complexes disappearance of the well defined band at 3412 cm^{-1} for enolic O—H stretching frequency (observed in the spectrum of the free ligand); clearly supports that on complexation the ligand (**LH**) undergoes deprotonation. The coordination of the deprotonated ligand to the metal centers in the respective complexes is also supported by the appearance of a strong C—O absorption band at 1094 (**1**), 1060 (**2**) and 1054 (**3**) cm^{-1}. The coordination of the heterocyclic nitrogen atom (pyridyl nitrogen of the deprotonated Schiff base ligand [**L**]$^-$) to the metal centers is evidenced by the low energy pyridine ring in-plane and out-of-plane vibrations in the spectrum of the **LH** (621 and 412 cm^{-1}), which in the spectra of the complexes shift to higher frequencies at 623, 641, 661 and 422, 430, 437 cm^{-1}, respectively [58]. Unlike the spectra of **1** and **3** an additional characteristic strong bifurcated absorption band is observed in the region 1060–1124 cm^{-1} for **2**, indicates the presence of perchlorate anions in the complex. Finally the coordination of the nitrogen atom to the metal center is evidenced by the appearance of the sharp ν_{M-N} bands obtained at 411 (**1**), 409 (**2**) and 406 (**3**) cm^{-1}, respectively.

3.2. UV–Vis spectroscopy

UV–Vis spectra of the ligand and the complexes (**1** and **2**) have been recorded at 300 K in HPLC grade acetonitrile solution but due to the poor solubility of **3** in acetonitrile medium, solid state Nujol mull absorption electronic spectrum was recorded for **3**. It has been already reported earlier [47] that the spectra of the free ligand (**LH**) shows two intraligand charge transfer (CT) bands at 331 and 248 nm whereas the spectra of all three complexes show three different CT bands at 450, 322, 266 nm (**1**), 402, 324, 258 nm (**2**) and 406, 328, 262 nm (**3**). Accordingly in **1**, **2** and **3** the bands obtained at 322, 266 nm, 324, 258 nm and 328, 262 nm are assigned to intraligand charge transfer transitions respectively but since the spectrum of the free ligand has no CT bands in the region 402–450 nm hence we can conclude that CT bands obtained at 450, 402 and 406 nm in **1**–**3**, respectively, are associated to L → M charge transfer transitions. Besides these allowed bands, the three compounds also show much weaker and less well defined broad

bands at 630 nm (**1**), 600 nm (**2**) and 634 and 682 nm (**3**) which are assigned to the d–d transitions in the respective complexes. The band at 630 nm for **1** is attributed $^1A_{1g} \rightarrow {}^1T_{1g}$ transition for the distorted octahedral cobalt(III) ion, whereas d–d transition at 600 nm for **2** is attributed to structurally well characterized square planar copper(II) complexes [59]. Unlike **1** and **2**, the two broad d–d bands obtained for **3** are in good agreement with the simultaneous presence of two different coordination environments in the complex. The band at 634 nm is associated with a copper(II) center having a distorted octahedral geometry and the d–d transition at 682 nm indicates the presence of copper(II) ions residing in a distorted square pyramidal geometry [60,61].

3.3. Structural description of the complexes

3.3.1. $[Co_2(\mathbf{L})_2(\mu_{1,1}\text{-}N_3)_2(N_3)_2]$ (**1**)

Complex **1** is a centrosymmetric *end-on* azido bridged cobalt(III) dinuclear species with a Co(1)···Co(1) separation of 3.127 Å (Fig. 1). The dinuclear unit is formed by two units of deprotonated NNO donor Schiff base ligands $[\mathbf{L}]^-$, two $\mu_{1,1}$-bridging azide ions and two terminally coordinated azide ions. The asymmetric unit forming the dinuclear unit is shown in Fig. 2. Bond lengths and angles of **1** are listed in Table 2. The cobalt center is six coordinated and presents a slightly distorted $[CoN_5O]$ octahedral geometry, mainly due to the coordination of the deprotonated NNO donor Schiff base ligand $[\mathbf{L}]^-$ and three azide ions (Fig. 1).

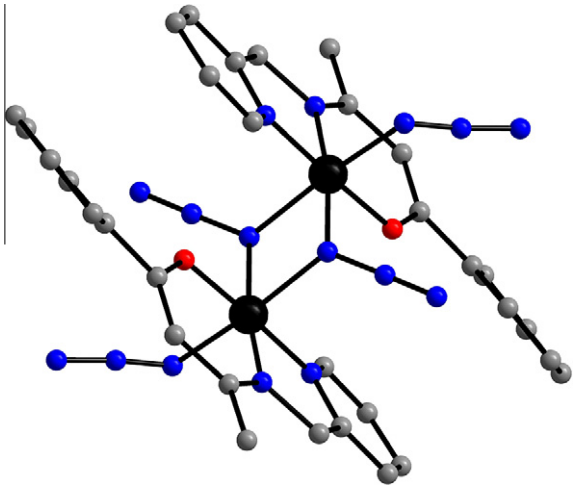

Fig. 1. μ-1,1-Azido bridged cobalt(III) dinuclear unit (**1**).

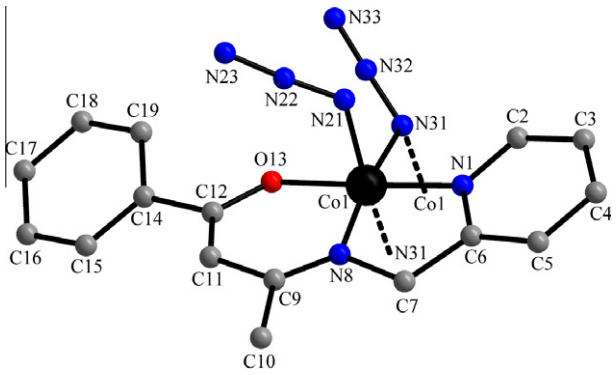

Fig. 2. Asymmetric unit of **1** with the atom labeling scheme.

Table 2
Selected bond lengths (Å) and angles (°) for **1**.

Bond lengths	(Å)
Co(1)–O(13)	1.869(5)
Co(1)–N(1)	1.922(7)
Co(1)–N(8)	1.886(6)
Co(1)–N(21)	1.921(9)
Co(1)–N(31)	1.999(6)
Co(1)–N(31)#1	2.024(7)
Bond angles	(°)
O(13)–Co(1)–N(1)	177.7(3)
O(13)–Co(1)–N(8)	94.9(3)
O(13)–Co(1)–N(21)	91.1(3)
O(13)–Co(1)–N(31)	87.2(3)
O(13)–Co(1)–N(31)#1	88.6(3)
N(1)–Co(1)–N(8)	85.1(3)
N(1)–Co(1)–N(21)	86.6(3)
N(1)–Co(1)–N(31)	93.2(3)
N(1)–Co(1)–N(31)#1	93.7(3)
N(8)–Co(1)–N(21)	94.3(3)
N(8)–Co(1)–N(31)	170.9(3)
N(8)–Co(1)–N(31)#1	93.2(3)
N(21)–Co(1)–N(31)	94.6(3)
N(21)–Co(1)–N(31)#1	172.6(3)
N(31)–Co(1)–N(31)#1	78.0(3)
Co(1)–O(13)–C(12)	125.3(5)
Co(1)–N(1)–C(2)	125.6(6)
Co(1)–N(1)–C(6)	115.4(5)
Co(1)–N(8)–C(7)	113.0(5)
Co(1)–N(8)–C(9)	126.0(6)
Co(1)–N(21)–N(22)	120.1(8)
Co(1)–N(31)–N(32)	117.6(5)
Co(1)–N(31)–Co(1)#1	102.0(3)
Co(1)#1–N(31)–N(32)	122.9(6)

Symmetry transformations used to generate equivalent atoms: #1 1 − *x*, −*y*, −*z*.

The equatorial sites of the two Co(1) centers are occupied by a deprotonated enolato oxygen atom of $[\mathbf{L}]^-$ and by thee nitrogen atoms: N(1), a pyridyl nitrogen of $[\mathbf{L}]^-$ and two azido nitrogen atoms: N(31), from a $\mu_{1,1}$-N_3 bridge and N(21), from a terminally coordinated azido ligand. The two axial sites of the cobalt(III) centers are occupied by two nitrogen atoms: an imine nitrogen, N(8), of the Schiff base ligand and the symmetry related N(31) atom of the second $\mu_{1,1}$-N_3 bridge. Thus the two cobalt(III) centers of the dimer are connected by two $\mu_{1,1}$-N_3 bridges that connect a basal position of one cobalt(III) ion with an axial position of the other and vice versa. Both azide ligands, (the terminal N21–N22–N23 and the bridging one, N31–N32–N33) are almost linear with N21–N22–N23 and N31–N32–N33 angles of 174.1(12)° and 178.3(9)°, respectively. The dimers are quite well isolated in the structure and do not present any H-bond (Fig. S1).

3.3.2. $[Cu_2(\mathbf{L})_2(\mu_{1,3}\text{-}N_3)]\cdot ClO_4$ (**2**)

Unlike the cobalt complex (**1**), **2** is a singly $\mu_{1,3}$-N_3 bridged copper(II) centro-symmetric dimer with the central N(4) atom of the $\mu_{1,3}$-N_3 bridge located on an inversion center. The copper(II) centers in **2** are four-coordinate, exhibiting a slightly distorted square-planar geometry, and present a CuN_3O environment formed by a pyridyl, N(1) and an imine nitrogen atom, N(2), both from $[\mathbf{L}]^-$, an azido nitrogen atom, N(3) of the $\mu_{1,3}$-bridging azide ligand and a deprotonated enolato oxygen atom, O(1) of $[\mathbf{L}]^-$ (in *trans* with the pyridyl N(1) atom, Fig. 3). The Cu–O bond distance is, as expected, shorter than the three Cu–N bond distances (Table 3). The overall N_2OCu–N_3–CuN_2O centro-symmetric dinuclear unit is almost perfectly planar, with a maximum deviation of only 0.06 Å from the average plane (Fig. 4). Furthermore, the complete dinuclear unit, including the Schiff base ligand, is also almost perfectly planar (Fig. 5). The charge neutrality of the complex $[Cu_2(\mathbf{L})_2(\mu_{1,3}\text{-}N_3)]^+$ is achieved by a perchlorate counter ion located

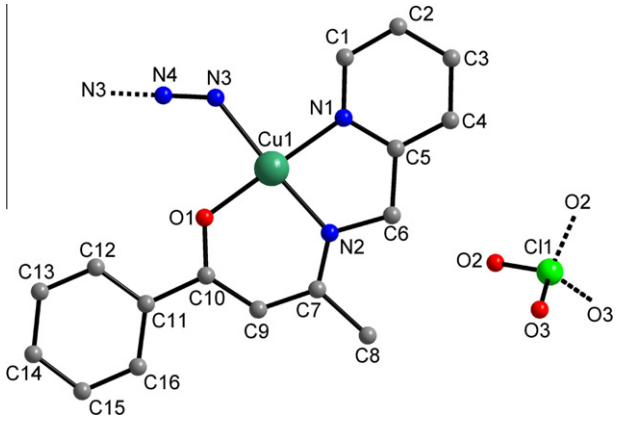

Fig. 3. Asymmetric unit of **2** with the atom labeling scheme.

Table 3
Selected bond lengths (Å) and angles (°) for **2.**

Bond lengths	(Å)
Cu(1)–O(1)	1.887(2)
Cu(1)–N(1)	1.983(2)
Cu(1)–N(2)	1.920(2)
Cu(1)–N(3)	2.009(2)
Bond angles	(°)
O(1)–Cu(1)–N(1)	177.79(10)
O(1)–Cu(1–N(2)	95.06(9)
O(1)–Cu(1)–N(3)	89.23(10)
N(1)–Cu(1)–N(2)	83.75(10)
N(1)–Cu(1)–N(3)	92.02(10)
N(2)–Cu(1)–N(3)	175.26(10)
Cu(1)–O(1)–C(10)	125.58(17)
Cu(1)–N(1)–C(1)	127.2(2)
Cu(1)–N(1)–C(5)	114.20(17)
Cu(1)–N(2)–C(7)	125.2(2)
Cu(1)–N(2)–C(6)	114.97(16)
Cu(1)–N(3)–N(4)	129.86(18)

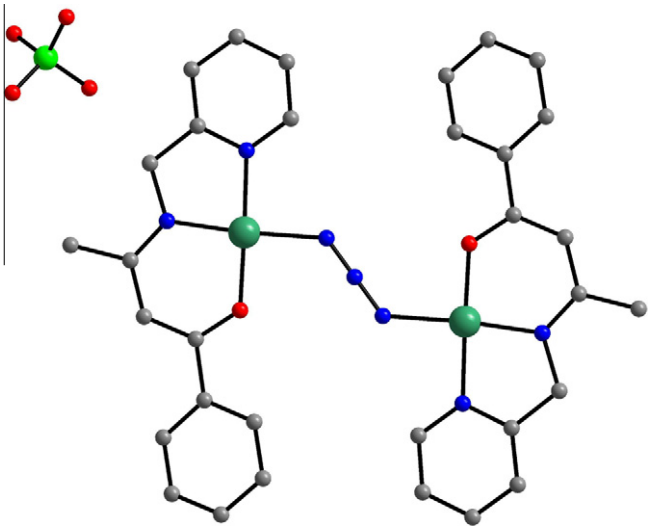

Fig. 4. μ-1,3-Azido bridged copper(II) dinuclear unit (**2**).

between the planar dimeric monocationic units. As in **1**, neither intra nor intermolecular H-bonding interactions are detected in **2**.

A search in the CCDC data base shows that **2** is the first singly $\mu_{1,3}$-N_3 bridged symmetrical, four coordinated, copper(II)–Schiff base dinuclear species [23–27]. The Cu(1)···Cu(1) separation in **2**

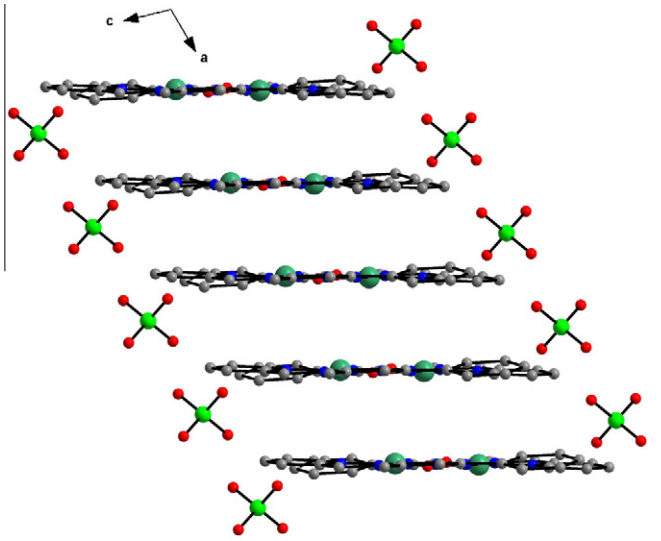

Fig. 5. Packing diagram of **2** showing the planarity of the dinuclear units along the *c*-axis and the lattice perchlorate ions.

is 5.789 Å and is shorter than that of the earlier reported copper(II) complexes with single $\mu_{1,3}$-N_3 bridges (6.086(7) Å) [21] but is similar to those of other copper(II) complexes with $\mu_{1,3}$-bridging cyanate (5.8 Å) and thiocyanate ligands (5.499 Å) [62]. As expected, the Cu(1)···Cu(1) separation in **2** is considerably longer than that typically observed in doubly $\mu_{1,3}$-N_3 bridged copper(II) species (5.264(1) Å) [63] since the two Cu(II) atoms are located in *trans* relative to the 1,3-azido bridge.

3.3.3. $[(\mu_{1,1}\text{-}N_3)_2Cu_5(\mu\text{-}O\mathbf{L})_2(\mu_{1,1}\text{-}N_3)_4(\mu_{1,1,1}\text{-}N_3)_2]_n$ (**3**)

X-ray crystal structure analysis shows that **3** $[Cu_5(\mu\text{-}O\mathbf{L})_2(\mu_{1,1}\text{-}N_3)_4(\mu_{1,1,1}\text{-}N_3)_2]^{2+}$ is a doubly $\mu_{1,1}$-azido bridged coordination polymer with $\mu_{1,1}$-azide ions connecting copper centers. The polymer is propagated along the *c* axis. Along the *c* axis copper bound Schiff base ligands alternate, related by 2-fold axes. The polymer is composed of vertex sharing defect dicubanes with one vertex unoccupied already seen [64,56]. Each dicubane is linked to the next via a symmetric double $\mu_{1,1}$-azido bridge link linking Cu(1) to its symmetry equivalent (Fig. 6). The bond lengths and angles for **3** are listed in Table 4. However, there are three distinct copper centers. Cu(1) is bound by four azido ligands but its fifth and longest contact is with the Schiff base enolato oxygen atom [O(1) = 2.486 Å forming a "long bond"]. Cu(2) is chelated by the tridentate NNO Schiff base with its fourth and fifth sites filled by a short bond of a $\mu_{1,1}$-bridging azide and a relatively "long bond" formed by a $\mu_{1,1,1}$-bridging azido ligand. Both five coordinate copper centers are square pyramidal but Cu(1) is more distorted towards trigonal bipyramidal geometry than Cu(2), as reflected in their Addison [65] parameters 0.22 and 0.03, respectively. Unlike Cu(1) and Cu(2), Cu(3) lies on a center of inversion, and is coordinated solely to azido ligands with typical Jahn-Teller distorted octahedral geometry (Fig. 7). The longest Cu–N contacts involves the triply bridging azido nitrogen [N(10)] and its symmetry equivalent. There are two unique double-bridging terminal azido ligands in the defect cubane, one, involving N(7), is significantly asymmetric, with the longer contact (2.025(2) Å) to Cu(3) and the shorter to Cu(1) (1.978(2) Å). The other azido N(13) bridges Cu(2) and Cu(3) in a symmetric fashion (2.031(2), 2.037(2) Å). The double azido bridge which links the cubanes is also symmetric but the Cu(1)–N distances are shorter: 1.990(2) Å to N(1) and 1.988(2) Å to N(4). The one unique triply bridging azido is quite asymmetric in the manner to which it binds to the three copper centers. Its closest contact is

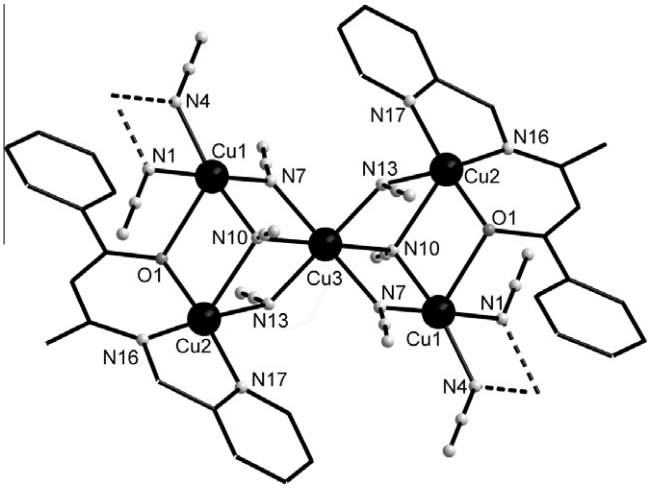

Fig. 6. μ-1,1 and μ-1,1,1-Azido bridged pentanuclear Cu_5 units of **3** showing the vacant cubane core. Symmetry code $-x, -y, -z+1$ relates the atoms generated by the center of inversion at Cu(3) of the asymmetric unit (half these labels need suffixes to denote the symmetry relationship).

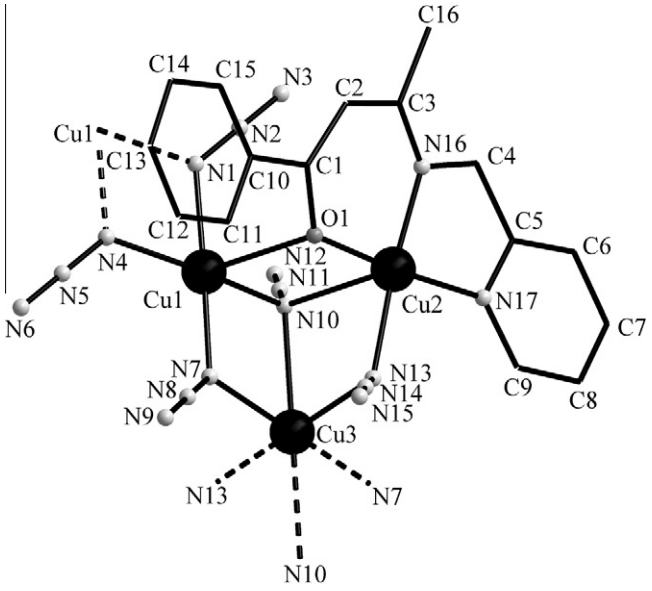

Fig. 7. Asymmetric unit of **3** with the atom labeling scheme.

Table 4
Selected bond lengths (Å) and angles (°) for **3**.

Bond lengths	*(Å)*	*Bond lengths*	*(Å)*
Cu(1)–N(7)	1.978(2)	Cu(3)–N(7)#1	2.025(2)
Cu(1)–N(4)	1.988(2)	Cu(3)–N(7)	2.025(2)
Cu(1)–N(1)	1.990(2)	Cu(3)–N(13)	2.037(2)
Cu(1)–N(10)	2.043(3)	Cu(3)–N(13)#1	2.037(2)
Cu(2)–O(1)	1.908(2)	Cu(3)–N(10)	2.455(3)
Cu(2)–N(16)	1.940(2)	Cu(3)–N(10)#1	2.455(3)
Cu(2)–N(17)	1.975(2)	N(1)–Cu(1)#2	1.990(2)
Cu(2)–N(13)	2.031(2)	N(4)–Cu(1)#2	1.988(2)
Bond angles	*(°)*	*Bond angles*	*(°)*
N(7)–Cu(1)–N(4)	99.93(11)	N(13)–Cu(3)–N(10)#1	97.63(8)
N(7)–Cu(1)–N(1)	175.38(9)	N(13)#1–Cu(3)–N(10)#1	82.37(8)
N(4)–Cu(1)–N(1)	76.65(11)	N(10)–Cu(3)–N(10)#1	180.0
N(7)–Cu(1)–N(10)	86.96(10)	N(2)–N(1)–Cu(1)#2	128.35(8)
N(4)–Cu(1)–N(10)	162.15(8)	N(2)–N(1)–Cu(1)	128.35(8)
N(1)–Cu(1)–N(10)	97.21(11)	Cu(1)#2–N(1)–Cu(1)	103.29(15)
O(1)–Cu(2)–N(16)	93.81(9)	N(5)–N(4)–Cu(1)	128.30(8)
O(1)–Cu(2)–N(17)	173.25(9)	N(5)–N(4)–Cu(1)#2	128.30(8)
N(16)–Cu(2)–N(17)	82.93(10)	Cu(1)–N(4)–Cu(1)#2	103.41(16)
O(1)–Cu(2)–N(13)	88.95(9)	N(8)–N(7)–Cu(1)	126.42(19)
N(16)–Cu(2)–N(13)	175.06(10)	N(8)–N(7)–Cu(3)	123.04(18)
N(17)–Cu(2)–N(13)	93.89(10)	Cu(1)–N(7)–Cu(3)	106.64(11)
N(7)#1–Cu(3)–N(7)	180.0	N(11)–N(10)–Cu(1)	120.34(19)
N(7)#1–Cu(3)–N(13)	89.94(10)	N(11)–N(10)–Cu(3)	130.9(2)
N(7)–Cu(3)–N(13)	90.06(10)	Cu(1)–N(10)–Cu(3)	90.61(11)
N(7)#1–Cu(3)–N(13)#1	90.06(10)	N(14)–N(13)–Cu(2)	115.56(18)
N(7)–Cu(3)–N(13)#1	89.94(10)	N(14)–N(13)–Cu(3)	114.3(2)
N(13)–Cu(3)–N(13)#1	180.0	Cu(2)–N(13)–Cu(3)	112.94(11)
N(7)#1–Cu(3)–N(10)	104.37(9)	C(3)–N(16)–Cu(2)	125.5(2)
N(7)–Cu(3)–N(10)	75.63(9)	C(4)–N(16)–Cu(2)	114.55(18)
N(13)–Cu(3)–N(10)	82.37(8)	C(9)–N(17)–Cu(2)	126.5(2)
N(13)#1–Cu(3)–N(10)	97.63(8)	C(5)–N(17)–Cu(2)	114.55(19)
N(7)#1–Cu(3)–N(10)#1	75.63(9)	C(1)–O(1)–Cu(2)	125.04(19)
N(7)–Cu(3)–N(10)#1	104.37(9)	–	–

Symmetry transformations used to generate equivalent atoms: #1 $-x, -y, -z+1$ #2 $-x, y, -z+1/2$.

with Cu(1) (2.043(3) Å) and its longest contact, rather longer than a conventional bond ("long bond"), is 2.570(3) Å to Cu(2) which is bound by the Schiff base and forms a long axial contact with respect to the square plane defined by the Schiff base and $\mu_{1,1}$-bridging azide N(13). Cu(2) is displaced by only 0.085 Å from this plane. In contrast N(1), N(4), N(7) and N(10) which bind Cu(1) cannot effectively be defined as one plane but rather as two, with the plane containing Cu(1), N(1) and N(4) inclined at 17.46° to the plane defined by Cu(1), N(7) and N(10). This also describes the twist of the polymeric bridge as it is propagated along the *c* axis (Fig. 8).

There are many hundreds of copper cubane structures in the CSD (version November 2009), but few involve predominantly N-binding ligands. Two structures in the CSD codes IBOBOQ [66] and RIZPAS [67] possess a Cu_3N_4 core and BIWVOT [68] has a Cu_3N_3O core which is closest to **3**. However, this core face-shares with its neighbor defect cubane as opposed to the vertex sharing found in **3**. The polymer in BIWVOT is propagated by double *end-to-end* azido bridges rather than the double *end-on* bridges as seen in **3**, which means that the cubane units are closer in **3** (3.121 Å) than in BIWVOT where the closest bridged Cu···Cu contact is 4.438 Å.

3.4. Magnetic properties

The thermal variation of the molar magnetic susceptibility per copper(II) dimer times the temperature ($\chi_m T$) for compound **2** shows at room temperature a value of ca. 0.50 emu K mol^{-1} (Fig. 9). This value is significantly lower than the expected one for two non interacting Cu^{II} $S = 1/2$ ions (0.75 emu K mol^{-1} for $g = 2.0$). When cooling down the sample, the $\chi_m T$ product shows a pronounced decrease to reach a plateau of ca. 0.01 emu K mol^{-1} at ca. 50 K. Below this temperature $\chi_m T$ remains constant and almost negligible down to 2 K (Fig. 9). This behavior indicates that compound **2** presents a strong antiferromagnetic coupling, as indicated by the low $\chi_m T$ value at room temperature and by the fact that the $\chi_m T$ plot shows a pronounced decrease starting above room temperature. As expected, this strong antiferromagnetic coupling leads to an $S = 0$ spin ground state. The very low $\chi_m T$ value observed at low temperatures comes from the presence of a small amount of paramagnetic impurity (probably as copper(II) monomers). This strong antiferromagnetic coupling is also confirmed in the thermal variation of the molar magnetic susceptibility (χ_m) that shows a broad maximum near room temperature (inset in Fig. 9). The paramagnetic impurity is also clearly observed as a Curie-type tail at low temperatures.

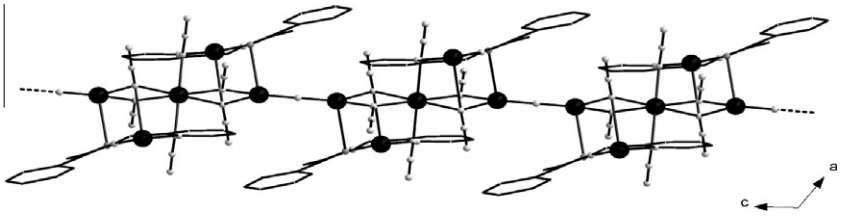

Fig. 8. 1D polymeric chain structure of **3** viewed along the *c* axis.

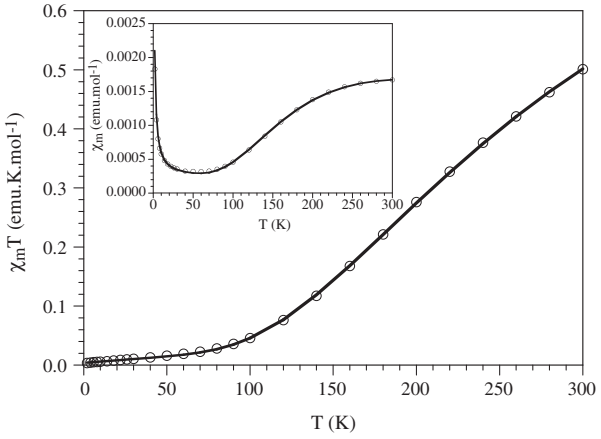

Fig. 9. Thermal variation of the $\chi_m T$ product per copper(II) dimer for **2**. Inset shows the thermal variation of the molar magnetic susceptibility, χ_m. Solid lines represent the best fit to the model (see text).

Since the structure of compound **2** shows the presence of Cu^{II} dimers with 1,3-N_3 (*end-to-end*) bridges, we have fit the magnetic properties to a simple Bleaney and Bowers $S = 1/2$ dimer model with an extra paramagnetic contribution arising from a small fraction of copper(II) monomers and a Nα term to account for the temperature independent paramagnetism (the Hamiltonian is written as $H = -JS_1S_2$): [69,70]

$$\chi = (1-c)\frac{2Ng^2\beta^2}{kT}\frac{1}{3+e^{-x}} + (c)\frac{Ng^2\beta^2}{2kT} + N\alpha, \quad \text{where } x = J/kT.$$

This model reproduces very satisfactorily the magnetic data of **2** in the whole temperature range with $g = 2.240(9)$, $J = -362(2)$ $K = -252(1)$ cm^{-1}, $N\alpha = 220 \times 10^{-6}$ emu mol^{-1} and $c = 0.4(1)\%$ (solid line in Fig. 9).

As expected, the magnetic coupling is strong and antiferromagnetic, in agreement with the magneto-structural correlations established for azide-bridged copper(II) complexes and with DFT calculations. These calculations show that the $\mu_{1,3}$-N_3 bridges give rise to strong antiferromagnetic interactions when the azide bridge connects equatorial positions in a square planar or square pyramidal geometry (Fig. S2) [9]. These calculations, performed for an ideal square pyramidal geometry, indicate that, given the structural parameters of **2**, the coupling should be very strong and antiferromagnetic, in agreement with the experimental value.

3.5. Catalytic studies

3.5.1. Catalytic properties of *1* for alkene oxidations

The ability of **1** to catalyze the oxidation of styrene was investigated using various oxidants including PhIO, H_2O_2, *m*-CPBA and O_2. O_2 was found not to be a good oxidant under conditions used here, but the complex showed to be an efficient catalyst for the styrene oxidation when PhIO is the oxidant. In Cl_2CH_2, the presence of 0.2 mol% **1** catalyze the oxidation of styrene with PhIO to yield 75% conversion in 3 h, and 90% conversion in 6 h (Table 5).

Analysis of the styrene oxidation profiles (Fig. 10) shows that **1** presents high selectivity towards the formation of styrene epoxide, yielding 83% of epoxide and 15% benzaldehyde. Addition of a neutral base, either NMO or PNO, has no effect on the styrene conversion or epoxide selectivity. Kinetic profiles show that benzaldehyde is mostly formed during the reaction course of epoxidation and is not due to subsequent oxidation of the styrene epoxide, but results from a reaction that takes place in parallel to styrene epoxidation. Fig. 10 also shows data obtained after a second addition of 500-times excess of styrene-PhIO over the catalyst left in the reaction mixture. The kinetic curves show that the styrene oxidation rate and epoxide selectivity after the second addition are essentially the same as in the first kinetic run. The fact that the catalyst retains its activity after successive additions evidences its robustness, affording turnover numbers as high as 900 (twice the t.o.n. of the first run). However, it must be noted that the electronic spectra taken at the end of the reaction differ from that of the starting complex, suggesting that **1** is a pre-catalyst that transforms into the active species upon reaction with the oxidant, the resting form of which differs from the starting complex.

When H_2O_2 was used as an oxygen source, the styrene oxidation catalyzed by **1** was found to be solvent dependent, being acetone better than Cl_2CH_2 or CH_3CN to carry out the catalysis. This is probably due to the formation of 2-hydroxy-2-hydroperoxypropane that stimulates gradual availability of the oxidant, limiting its decomposition [71,72]. In acetone, catalyst **1** converted 34% of styrene in 4 h. It is evident from Table 5 that between H_2O_2 and PhIO, the later acts as a better oxidant with respect to both styrene conversion and epoxide selectivity. The lower efficiency of the complex to catalyze the epoxidation of styrene with H_2O_2 can be attributed to catalyst deactivation in aqueous medium and partial H_2O_2 disproportionation. Also in this case, addition of a neutral donor ligand (NMO or PNO) showed no effect on the styrene conversion or epoxide selectivity. When 0.2 mol% of **1** was used, no catalytic effect was observed on the rate of styrene oxidation with *m*-CPBA at 0 °C. However, after increasing the proportion of catalyst in the reaction mixture to 4 mol% (catalyst:styrene:*m*-CPBA = 1:25:50), styrene was catalytically oxidized by the *m*-CPBA-**1** system (Table 6). With this oxidant, it was found that the styrene oxidation in CH_3CN gave superior yield in a time shorter than in CH_2Cl_2. The **1**-*m*-CPBA system was further explored in CH_3CN for the other alkenes listed in Table 6. As it can be observed, oxidation rates of cyclohexene and *trans*-4-octene are faster than those of styrene and *cis*-stylbene, which indicates that the catalyst favors the oxidation of the more electron rich substrates over the less ones. This result would suggest an electrophilic character for the active site of catalyst. However, given that a similar trend is found for the oxidation of these alkenes with *m*-CPBA alone – although at a much slower rate –, this interpretation should be taken with care.

It is interesting to compare the catalytic performance of **1** with that of other Co-based systems. Complexes of the Co-salen family have been reported to catalyze the epoxidation of cyclohexene with PhIO in Cl_2CH_2 at 25 °C, to yield 66% conversion (t.o.n. = 6.6)

Table 5
Catalytic oxidation of styrene with **1**.

1 (μmol)	Solvent	Styrene (mmol)	Oxidant (mmol)	Time (h)	*T* (°C)	t.o.n.	Conversion (%)	Epoxide (%)
1	CH_2Cl_2[a]	0.5	PhIO (1)	6	20	450	90	83
1	Acetone[b]	0.5	H_2O_2 (5)	4	0	170	34	59

[a] 5 mL.
[b] 1 mL. t.o.n. = converted mol/mol metal catalyst.

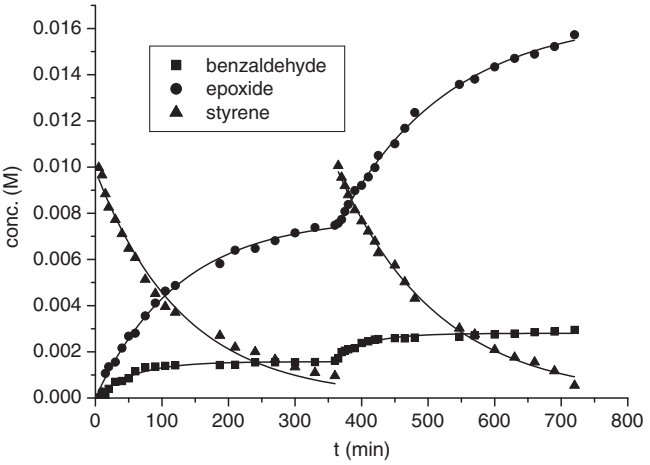

Fig. 10. Reaction profiles of the styrene oxidation with PhIO catalyzed by **1** in Cl_2CH_2, at 20 °C. Experimental conditions: 0.5 mmol styrene, 1 mmol PhIO, 0.2 mol% catalyst, 5 mL CH_2Cl_2. Second addition of 0.5 mmol styrene + 1 mmol PhIO at *t* = 360 min.

Table 6
Oxidation of alkenes with *m*-CPBA catalyzed by **1**, at 0 °C.

Alkene	Solvent	Time (h)	Conversion (%)
Styrene	CH_2Cl_2	5	67
	CH_3CN	3	95
Cis-stylbene	CH_3CN	3	94
Cyclohexene	CH_3CN	$\ll 1$[a]	99
Trans-4-octene	CH_3CN	$\ll 1$[a]	98

Reaction conditions: alkene (0.5 mmol), catalyst (20 μmol), *m*-CPBA (1 mmol), solvent (1 mL).
[a] The first aliquot taken a few minutes after the reaction started showed maximal conversion.

in 2 h [73]. Other Co complexes of the same family were found to yield 35 mol% of styrene epoxide (t.o.n. = 7) in 3.5 h, in DMF and 0 °C, when H_2O_2 was used as terminal oxidant [74]. Co-calix [57] pyrrole complexes were found to catalyze styrene epoxidation by O_2/ethylbutyraldehyde with 68% of epoxide formation (t.o.n. = 68), after 24 h [75]. In all these systems, the catalysts are used in high proportion and low t.o.n. are achieved. An improved catalytic system for cyclohexene oxidation was obtained with a heterogeneous system: LDH-hosted Co-salen complex, which yields 53% of epoxide (t.o.n. = 98) using O_2/aldehyde as oxidant [76].

Therefore, although less active for epoxidation of alkenes than Mn catalysts [77–81], the high turnover numbers and the retention of activity after successive additions of oxidant, places the catalytic activity of the **1**-PhIO system above those of other cobalt catalysts reported so far for alkene oxidation in homogeneous phase.

3.5.2. Catalase-like activity studies for ***2***

The catalase-like function of **2** to disproportionate H_2O_2 into H_2O and O_2 was examined at 0 and 25 °C by volumetric measurements of evolved dioxygen. The complex **2** was insoluble in water therefore, catalytic activities of the complexes were determined in *N*,*N*-dimethylformamide. Experiments were repeated several times to ensure consistency of the results. The time course of the dioxygen evolution is shown in Fig. 11. The reactivity studies indicated that the complex itself is catalytically almost inactive, but the decomposition of H_2O_2 is enhanced in the presence of a base such as 1-methylimidazole (1-MeimH), imidazole (imH) or pyridine (py) because of their strong π-donating ability. However, it is observed that base itself causes only a very slight disproportionation of the peroxide. For **2**, the dioxygen evolution rate was reached after the reaction was initiated and the evolution profile followed by a short slow period process to finish the reaction. When the catalytic process ceased, the evolved dioxygen gas corresponds to 100% decomposition of hydrogen peroxide, implying that the complex catalysts are efficient towards peroxide dismutation.

When studied at 0 °C the oxygen evolution profile was sigmoidal and evolution ceased in 17 min. On the other hand, the catalysis became faster and the evolution ceased in 8 min at 25 °C. At this stage the evolved dioxygen corresponded to 100% decomposition of the added hydrogen peroxide (Fig. 12). Different concentrations are tested for heterocyclic base and H_2O_2 to find optimal ratio (Fig. 13). By observing the profiles, we can find that the maximum catalytic activities occur near the point where the concentrations of imidazole are equal to that of H_2O_2. The same result was observed when 1-methylimidazole or pyridine was used instead of imidazole. But it was found that 1-methylimidazole appears to be the most efficient base for peroxide disproportionation. This fact means the catalytic activity of the complex is related with the pKa of the added heterocyclic base, indicating that the ability of 1-methylimidazole for binding proton is larger than that of imidazole and pyridine [82]. This is also consistent with the pKa of pyridine (5.2), imidazole (7.1) and 1-methylimidazole (7.4).

The catalytic results indicate that **2** has reasonably good catalase activity and may be suitable as a functional model for the pseudocatalase enzyme.

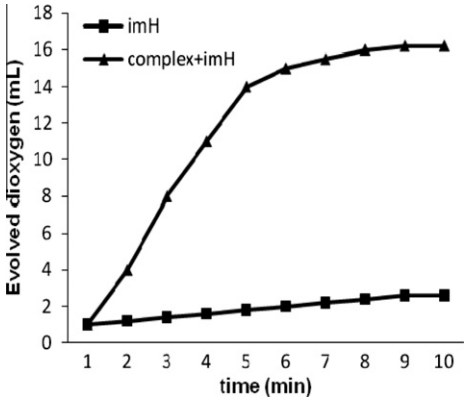

Fig. 11. Time-course profiles of dioxygen evolution (mL) from the reaction of H_2O_2 (1 mL, 30 %) with: (■) just imidazole (0.5 mL) and (▲) **2** (2 mL, 1 mM) with imidazole (0.5 mL) in DMF at 25 °C.

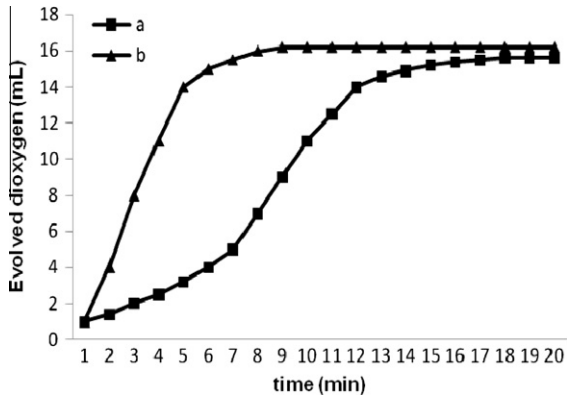

Fig. 12. Time-course profiles of dioxygen evolution (mL) from the reaction of H_2O_2 (1 mL, 30%) with: **2** (2 mL, 1 mM) and imidazole (0.5 mL) in DMF at (a) 0 °C and (b) 25 °C.

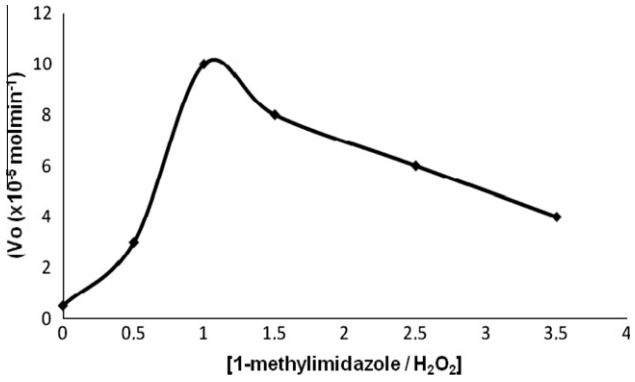

Fig. 13. Plot of initial rates of dioxygen evolution vs. the concentration ratios of 1-methylimidazole to H_2O_2.

*3.5.3. Effect of **2** on catalase activity of haemolysate*

The effect of **2** on catalase activity of haemolysate to disproportionate H_2O_2 into H_2O and O_2 was examined in *N*,*N*-dimethylformamide at room temperature. The catalytic activity of haemolysate was investigated in the presence and absence of the complex. The catalase activity of the control group changes significantly in the experimental group but the catalytic degradation of H_2O_2 is inhibited by the complex (Fig. S3). This result may be due to $\mu_{1,3}$-azido bridges of the complex. Because it is known that the activity of catalase is inhibited by several compounds, including its natural substrate, H_2O_2 (concentrations >0.1 M and reaction times >30 s), azide, acetic acid, formic acid, fluoride, cyanide, hydroxylamine, carbon monoxide, heavy metals (Cu^{2+}, Pb^{2+}) and 3-amino-1,2,4-triazine [83–85].

The interesting aspect of **2** is that in spite of $\mu_{1,3}$-bridging azido ligand, it exhibits catalytic activity and catalyses the disproportionation of hydrogen peroxide in presence of added base, as observed in the literature [86]. On the other hand, it is found that at pH 7.4 and in presence of excess hydrogen peroxide the catalytic activity of blood haemolysate is inhibited by the complex.

Moreover, the effect of complex concentration on the degradation of H_2O_2 by haemolysate has been investigated. For this purpose the hydrogen peroxide concentration is kept constant and the concentration of **2** is varied (1–40 mM). It was found that inhibition of blood haemolysate increases with the increasing of the complex concentrations (Fig. S4). Thus, at low complex concentrations the inhibition of haemolysate varies linearly with the complex concentration, but over 5 mM complex concentrations, inhibition of blood haemolysate by the complex is increasing slightly.

4. Conclusion

Three new cobalt(III) and copper(II) complexes, formulated as $[Co_2(\mathbf{L})_2(\mu_{1,1}\text{-}N_3)_2(N_3)_2]$ (**1**), $[Cu_2(\mathbf{L})_2(\mu_{1,3}\text{-}N_3)].ClO_4$ (**2**) and $[(\mu_{1,1}\text{-}N_3)_2Cu_5(\mu\text{-}O\mathbf{L})_2(\mu_{1,1}\text{-}N_3)_4(\mu_{1,1,1}\text{-}N_3)_2]_n$ (**3**) have been synthesised with the tridentate NNO donor Schiff base ligand [(1*Z*,3*E*)-3-((pyridin-2-yl)methylimino)-1-phenylbut-1-en-1-ol = **LH**] and azide ions. Interestingly, **2** is the first dinuclear copper(II) square planar complex with a tridentate Schiff base and a single $\mu_{1,3}$-azido bridge. Another intriguing fact in this complex is the presence of a very strong antiferromagnetic exchange interaction ($J = -252(1)\ cm^{-1}$) through the single $\mu_{1,3}$-azido bridge. This value is more than twice the highest value reported to date for a double $\mu_{1,3}$-azido bridged copper(II)-dinuclear compound ($J = -105\ cm^{-1}$) [21]. Last, but not the least, the high turnover numbers and the retention of activity after successive additions of oxidant, places the catalytic activity of the **1**-PhIO system above those of other cobalt catalysts reported so far for alkene oxidation in homogeneous phase and **2** have shown to have reasonably good catalase activity.

Acknowledgements

A. Ray is thankful to the Council of Scientific and Industrial Research New Delhi, Govt. of India for providing her the financial support to carry out the work. Professor L.K. Thompson and Dr. L.N. Dawe, Department of Chemistry, Memorial University, St. John's, NL, A1B 3X7, Canada, are thanked for structural and variable temperature magnetic data on **2**. We also thank the European Union (MAGMANet), the Spanish Ministerio de Educación y Ciencia (Projects MAT2007-61584 and CSD 2007-00010 Consolider-Ingenio in Molecular Nanoscience) and the Generalitat Valenciana (Project PROMETEO/2009/095) for financial assistance.

Appendix A. Supplementary material

CCDC 678481, 678482, 649739 contains the supplementary crystallographic data for complexes **1**, **2** and **3**, respectively. These data can be obtained free of charge from The Cambridge Crystallographic Data Centre via www.ccdc.cam.ac.uk/data_request/cif. Supplementary data associated with this article can be found, in the online version, at doi:10.1016/j.ica.2011.04.008.

References

[1] M.W. Wemple, D.M. Adams, K.S. Hagen, K. Folting, D.N. Hendrickson, G. Christou, Chem. Commun. (1999) 1591.
[2] A.K. Boudalis, B. Donnadieu, V. Nastopoulos, J. Modesto Clemente-Juan, A. Mari, Y. Sanakis, J.-P. Tuchagues, S.P. Perlepes, Angew. Chem., Int. Ed. 43 (2004) 2266.
[3] F. Meyer, S. Demeshko, G. Leibeling, B. Kersting, E. Kaifer, H. Pritzkow, Chem.–Eur. J. 11 (2005) 518.
[4] S. Demeshko, G. Leibeling, W. Maringgele, F. Meyer, C. Mennerich, H.H. Klauss, H. Pritzkow, Inorg. Chem. 44 (2005) 519.
[5] J. Ribas, A. Escuer, M. Monfort, R. Vicente, R. Cortés, L. Lezama, T. Rojo, Coord. Chem. Rev. 195 (1999) 1027.
[6] M.A.M. Abu-Youssef, A. Escuer, M.A.S. Goher, F.A. Mautner, G.J. Reiss, R. Vicente, Angew. Chem., Int. Ed. 39 (2000) 1621.
[7] A. Escuer, F.A. Mautner, M.A.S. Goher, M.A.M. Abu-Youssef, R. Vicente, Chem. Commun. (2005) 605.
[8] E. Ruiz, J. Cano, S. Alvarez, P. Alemany, J. Am. Chem. Soc. 120 (1998) 122.
[9] F. Fabrizi de Biani, E. Ruiz, J. Cano, J.J. Novoa, S. Alvarez, Inorg. Chem. 39 (2000) 3221.
[10] S. Triki, C.J. Gómez-García, E. Ruiz, J. Sala-Pala, Inorg. Chem. 44 (2005) 496.
[11] M.I. Arriortua, A.R. Cortes, L. Lezema, T. Rojo, X. Solans, Inorg. Chim. Acta 174 (1990) 263.
[12] A. Escuer, R. Vicente, J. Ribas, X. Solans, Inorg. Chem. 34 (1995) 1793.
[13] A. Escuer, M.A.S. Goher, F.A. Mautner, R. Vicente, Inorg. Chem. 39 (2000) 2107.

[14] J. Comarmond, P. Plumere, J.M. Lehn, Y. Agnus, R. Louis, R. Weiss, O. Kahn, I. Morgesten-Badarau, J. Am. Chem. Soc. 104 (1982) 6330.
[15] O. Kahn, S. Sikorav, J. Gouteron, S. Jeannin, Y. Jeannin, Inorg. Chem. 22 (1983) 2877.
[16] L. Zhang, J.-L. Zuo, S. Gao, Y. Song, C.-M. Che, H.-K. Fun, X.-Z. You, Angew. Chem., Int. Ed. 39 (2000) 3633.
[17] B. Graham, M.T.W. Hearn, P.C. Junk, C.M. Kepert, F.E. Mabbas, B. Moubaraki, K.S. Murray, L. Spiccia, Inorg. Chem. 40 (2001) 1536.
[18] P. Manikandan, R. Muthukumaran, K.R. Justin Thomas, B. Varghese, G.V.R. Chandramouli, P.T. Manoharan, Inorg. Chem. 40 (2001) 2378.
[19] S. Shit, P. Talukder, J. Chakraborty, G. Pilet, M. Salah El Fallah, J. Ribas, S. Mitra, Polyhedron 26 (2007) 1357.
[20] A. Escuer, M. Font-Bardía, S.S. Massoud, F.A. Mautner, E. Peñalba, X. Solans, R. Vicente, New J. Chem. 28 (2004) 681.
[21] S. Sarkar, A. Mondal, J. Ribas, M.G.B. Drew, K. Pramanik, K.K. Rajak, Inorg. Chim. Acta 358 (2005) 641.
[22] Y. Xie, Y.Q. Liu, H. Jiang, C. Du, X. Xu, M. Yu, Y. Zhu, New J. Chem. 26 (2002) 176.
[23] A.M. Madalan, M. Noltemeyer, M. Neculai, H.W. Roesky, M. Schmidtmann, A. Müller, Y. Journaux, M. Andruh, Inorg. Chim. Acta 359 (2006) 459.
[24] K. Matsumoto, S. Ooi, K. Nakatsuka, W. Mori, S. Suzuki, A. Nakahara, Y. Nakao, J. Chem. Soc., Dalton Trans. (1985) 2095.
[25] P. Chaudhuri, K. Oder, K. Wieghardt, B. Nuber, J. Weiss, Inorg. Chem. 25 (1986) 2818.
[26] I. Murase, I. Ueda, N. Marubayashi, S. Kida, N. Matsumoto, M. Kudo, M. Toyohara, K. Hiate, M. Mikuriya, J. Chem. Soc., Dalton Trans. (1990) 2763.
[27] Y.-Qian Cheng, M.-Lin Hu, S. Wang, M.-De Ye, Acta Crystallogr., Sect.C: Cryst. Struct. Commun. 58 (2002) m12.
[28] Z. Xi, H. Wang, Y. Sun, N. Zhou, G. Cao, M. Li, J. Mol. Catal. A: Chem. 168 (2001) 299.
[29] T. Mykaiyama, T. Yamada, Bull. Chem. Soc. Jpn. 68 (1995) 17.
[30] P. Mastrorilli, C.F. Nobile, G.P. Surana, L. Lopez, Tetrahedron 51 (1995) 7943.
[31] I. Ferhadeze, J.R. Petro, R. de la Salud, Tetrahedron 52 (1996) 12031.
[32] K.S. Ravikumar, F. Barber, J.P. Bugui, D. Bonnet-Dolpon, Tetrahedron 54 (1998) 7457.
[33] E.N. Jacobsen, F. Kakiuchi, R.G. Konsler, J.F. Larrow, M. Tokunaga, Tetrahedron Lett. 38 (1997) 773.
[34] M.H. Wu, E.N. Jacobson, Tetrahedron Lett. 38 (1997) 1693.
[35] D.E. De Vos, P.P. Knops-Gerrits, D.L. Vanoppen, P.A. Jacobs, Supramol. Chem. 6 (1995) 49.
[36] D. Chatterjee, S. Mukherjee, A. Mitra, J. Mol. Catal. A: Chem. 154 (2000) 5.
[37] Y.-Yong Yan, W. Yang, T.-Jun Wang, M.-Yu Huang, Y.-Yan Jiang, Polym. Adv. Technol. 7 (1996) 729.
[38] B. Dede, F. Karipcin, M. Cengiz, J. Hazard. Mater. 163 (2009) 1148.
[39] M. Zamocky, F. Koller, Prog. Biophys. Mol. Biol. 72 (1999) 19.
[40] X. Chen, H. Xie, J. Kong, J. Deng, Biosens. Bioelectron. 16 (2001) 115.
[41] I. Fridovich, Annu. Rev. Biochem. 64 (1995) 97.
[42] S. Choua, P. Pacheco, C. Coquelet, E. Bienvenue, J. Inorg. Biochem. 65 (1997) 79.
[43] J. Gao, A.E. Martell, J.H. Reibenspies, Inorg. Chim. Acta 346 (2003) 32.
[44] A.E.M. Boelrijk, G.C. Dismukes, Inorg. Chem. 39 (2000) 3020.
[45] J. Paschke, M. Kirsch, H.-G. Korth, H. Groot, R. Sustmann, J. Am. Chem. Soc. 123 (2001) 11099.
[46] J. Gao, J. Reibenspies, A.E. Martell, S. Yizhen, D. Chen, Inorg. Chem. Commun. 5 (2002) 1095.
[47] A. Ray, G. Pilet, C.J. Gómez-García, S. Mitra, Polyhedron 28 (2009) 511.
[48] H. Saltzman, J.G. Sharefkin, Org. Synth., Wiley, New York, 1973, Collect. Vol. V, p. 658.
[49] G. Cascarano, A. Altomare, C. Giacovazzo, A. Guagliardi, A.G.G. Moliterni, D. Siliqi, M.C. Burla, G. Polidori, M. Camalli, Acta Crystallogr., Sect. A 52 (1996) C.
[50] D.J. Watkin, C.K. Prout, J.R. Carruthers, P.W. Betteridge, CRYSTALS, Chemical Crystallography Laboratory, Oxford, UK, 1999.
[51] R.H. Blessing, Acta Crystallogr., Sect. A 51 (1995) 33.
[52] G.M. Sheldrick, SHELXS-97, Program for Crystal Structure Refinement, University of Göttingen, Göttingen, 1990.
[53] G.M. Sheldrick, SHELXL-97, Program for Crystal Structure Refinement, University of Göttingen, Göttingen, 1997.
[54] APEX2, Version 2.1, SMART, SAINT, SADABS, XPREP, XS, XL, XP, Bruker AXS Inc., Madison, Wisconsin, USA, 2004–2006.
[55] P. Ninfali, T. Orsenigo, L. Barociani, S. Rapa, Prep. Biochem. 20 (1990) 297.
[56] P. Mukherjee, M.G.B. Drew, M. Estrader, C. Diaz, A. Ghosh, Inorg. Chim. Acta 361 (2008) 161.
[57] S. Dalai, P.S. Mukherjee, M.G.B. Drew, T.-H. Lu, N. Ray Chaudhuri, Inorg. Chim. Acta 335 (2002) 85.
[58] K. Nakamoto, Infrared and Raman Spectra of Inorganic and Coordination Compounds, fifth ed., vol. 23, Wiley, New York, 1997.
[59] A.B.P. Lever, Inorganic Electronic Spectroscopy, Elsevier, Amsterdam, 1984. p. 553.
[60] F.A. Cotton, G.A. Wilkinsons, Advanced Inorganic Chemistry, fourth ed., Wiley-Interscience Publication, 1980. p. 816.
[61] J.P. Costes, J.P. Laurent, J.M.M. Sanchez, J.S. Varela, M. Ahlgren, M. Sundberg, Inorg. Chem. 36 (1997) 4641.
[62] P. Talukder, A. Datta, S. Mitra, G. Rosair, M.S. El Fallah, J. Ribas, Dalton Trans. (2004) 4161.
[63] S.S. Massoud, F.A. Mautner, Inorg. Chim. Acta 358 (2005) 3334.
[64] W.S. Han, S.W. Lee, Dalton Trans. (2004) 3360.
[65] A.W. Addison, T.N. Rao, J. Reedijk, J. van Rijn, G.C. Verschoor, J. Chem. Soc., Dalton Trans. (1984) 1349.
[66] P. Roy, K. Dhara, M. Manassero, P. Banerjee, Inorg. Chem. Commun. 11 (2008) 265.
[67] L. Zhang, L.-Fu Tang, Z.-Hong Wang, M. Du, M. Julve, F. Lloret, J.-Tao Wang, Inorg. Chem. 40 (2001) 3619.
[68] K.C. Mondal, P.S. Mukherjee, Inorg. Chem. 47 (2008) 4215.
[69] B. Bleaney, K.D. Blowers, Proc. Roy. Soc. (London) Ser. A 214 (1952) 451.
[70] O. Kahn, Molecular Magnetism, VCH Publishers, 1993.
[71] É. Balogh-Hergovich, G. Speier, J. Mol. Cat. A: Chem. 230 (2005) 79.
[72] P. Knops-Gerrits, D. De Vos, P. Jacobs, J. Mol. Cat. A: Chem. 117 (1997) 57.
[73] J.D. Koola, J.K. Kochi, J. Org. Chem. 52 (1987) 4545.
[74] X.H. Lu, Q.H. Xia, H.J. Zhan, H.X. Yuan, C.P. Ye, K.X. Su, G. Xu, J. Mol. Cat. A: Chem. 250 (2006) 169.
[75] P. Buranaprassertsuk, Y. Tangsakol, W. Chavasiri, Cat. Commun. 8 (2007) 310.
[76] S. Bhattacharjee, T.J. Dines, J.A. Anderson, J. Phys. Chem. C 112 (2008) 14124.
[77] M. Palucki, P.J. Pospisil, W. Zhang, E.N. Jacobsen, J. Am. Chem. Soc. 116 (1994) 9333.
[78] K. Srinivasan, P. Michaud, J.K. Kochi, J. Am. Chem. Soc. 108 (1986) 2309.
[79] J.P. Collman, L. Zeng, J.I. Brauman, Inorg. Chem. 43 (2004) 2672.
[80] S. Majumder, S. Hazra, S. Dutta, P. Biswas, S. Mohanta, Polyhedron 28 (2009) 2473.
[81] A.R. Silva, C. Freire, B. de Castro, New J. Chem. 28 (2004) 253.
[82] J.J. Zhang, Q.H. Luo, C.Y. Duan, Z.L. Wang, H. Mei, J. Inorg. Biochem. 86 (2001) 573.
[83] H.N. Kirkman, S. Galiano, G.F. Gaetani, J. Biol. Chem. 262 (1987) 660.
[84] H.N. Kirkman, M. Rolfo, A.M. Ferraris, G.F. Gaetani, J. Biol. Chem. 274 (1999) 13908.
[85] G.R. Schonbaum, B. Chance, Catalase. The Enzymes, in; P.D. Boyer (Ed.), Academic Press, New York, 1976, vol. 13, p. 363.
[86] U.P. Singh, P. Tyagi, S. Upreti, Polyhedron 26 (2007) 3625.